Published in final edited form as:

J Vasc Interv Radiol. 2022 July ; 33(7): 764–774.e4. doi:10.1016/j.jvir.2022.03.026.

Impact of Chemoembolic Regimen on Immune Cell Recruitment and Immune Checkpoint Marker Expression following Transcatheter Arterial Chemoembolization in a VX2 Rabbit Liver Tumor Model

Antonia M. Berz, MS,

Jessica G. Santana, MSc,

Simon Iseke, MS,

Moritz Gross, MS,

Vasily Pekurovsky, BSc,

Fabian Laage Gaupp, MD,

Lynn J. Savic, MD,

Tabea Borde, MD,

Luzie A. Gottwald, MD,

Anne Marie Boustani, MD,

Bernhard Gebauer, MD,

MingDe Lin, PhD,

Xuchen Zhang, MD, PhD,

Todd Schlachter, MD,

David C. Madoff, MD,

Julius Chapiro, MD, PhD

Department of Radiology and Biomedical Imaging (A.M.Be., J.G.S., S.I., M.G., V.P., F.L-G., L.J.S., A.M.Bo., M.L., T.S., D.C.M., J.C.), Department of Pathology (X.Z.), and Department of Internal Medicine (D.C.M.), Yale School of Medicine, New Haven, Connecticut; Charité–Universitätsmedizin Berlin, corporate member of Freie Universität Berlin and Humboldt-Universität zu Berlin, Department of Radiology (A.M.Be., M.G., L.J.S., T.B., L.A.G., B.G.) Berlin, Germany; Department of Diagnostic and Interventional Radiology (S.I.), Pediatric Radiology and Neuroradiology, Rostock University Medical Center, Rostock, Germany; Berlin Institute of Health at Charité–Universitätsmedizin Berlin (L.J.S.), Berlin, Germany; and Visage Imaging, Inc. (M.L.), San Diego, California.

Abstract

Address corresponding to J.C., Department of Radiology and Biomedical Imaging, Yale University School of Medicine, 300 Cedar Street, the Anlyan Center, N312A, New Haven, CT 06520; julius.chapiro@yale.edu.

From the RSNA Annual Meeting 2021, Abstract Number: SP-12515 - “Impact of Chemo-Embolic Choice on the Tumor Microenvironment and Local Immune Response to Transarterial Chemoembolization in a VX2 Rabbit Liver Tumor Model.”

Figures E1–E3, Table E1, and Appendix A can be found by accessing the online version of this article on www.jvir.org and selecting the Supplemental Material tab.

Purpose: To characterize the effects of commonly used transcatheter arterial chemoembolization (TACE) regimens on the immune response and immune checkpoint marker expression using a VX2 rabbit liver tumor model.

Materials and Methods: Twenty-four VX2 liver tumor-bearing New Zealand white rabbits were assigned to 7 groups (n = 3 per group) undergoing locoregional therapy as follows: (*a*) bicarbonate infusion without embolization, (*b*) conventional TACE (cTACE) using a water-in-oil emulsion containing doxorubicin mixed 1:2 with Lipiodol, drug-eluting embolic-TACE with either (*c*) idarubicin-eluting Oncozene microspheres (40 μm) or (*d*) doxorubicin-eluting Lumi beads (40–90 μm). For each therapy arm (*b*–*d*), a tandem set of 3 animals with additional bicarbonate infusion before TACE was added, to evaluate the effect of pH modification on the immune response. Three untreated rabbits served as controls. Tissue was harvested 24 hours after treatment, followed by digital immunohistochemistry quantification (counts/μm^2 ± SEM) of tumor-infiltrating cluster of differentiation 3^+ T-lymphocytes, human leukocyte antigen DR type antigen-presenting cells (APCs), cytotoxic T-lymphocyte–associated protein-4 (CTLA-4), and programmed cell death protein-1 (PD-1)/PD-1 ligand (PD-L1) pathway axis expression.

Results: Lumi-bead TACE induced significantly more intratumoral T-cell and APC infiltration than cTACE and Oncozene-microsphere TACE. Additionally, tumors treated with Lumi-bead TACE expressed significantly higher intratumoral immune checkpoint markers compared with cTACE and Oncozene-microsphere TACE. Neoadjuvant bicarbonate demonstrated the most pronounced effect on cTACE and resulted in a significant increase in intratumoral cluster of differentiation 3^+ T-cell infiltration compared with cTACE alone.

Conclusions: This preclinical study revealed significant differences in evoked tumor immunogenicity depending on the choice of chemoembolic regimen for TACE.

In Western populations, hepatocellular carcinoma (HCC) most commonly arises from a background of chronic liver inflammation (1). In this setting, HCC utilizes the hyperglycolytic tumor microenvironment (TME), aggravated by tissue acidosis, to escape from the immune system (1–3). This hostile yet permissive microenvironment represents a hallmark of tumor resistance in which all T-cell effector properties are suppressed (2,3). The metabolic shift within the TME renders T-cells sensitive to negative regulatory signals by the upregulation of cytotoxic T-lymphocyte–associated protein-4 (CTLA-4) and programmed cell death protein-1 (PD-1) enhancing tumor immune tolerance by the overexpression of PD-1 ligands (PD-L1) (2–4). Such a scenario enables tumor cells to circumvent an effective immune response and to promote their growth and survival (3,4).

Catheter-based locoregional therapy (LRT) with transcatheter arterial chemoembolization (TACE) is the well-established standard of care in patients with intermediate-stage HCC (5). Although conventional TACE (cTACE) with Lipiodol is the only guideline-approved therapy, numerous drug-eluting embolic (DEE)–based options have been developed and are widely used (5–7). Both cTACE and DEE-TACE are frequently used inter-changeably, including in clinical trials investigating the combination of TACE with systemic therapy (8,9). The recent advent of various systemic immunotherapies and the Food and Drug Administration (FDA) approval for HCC has generated interest in combining those targeted therapies with TACE (10). Along these lines, the main mechanistic goal of any such

combination therapy is to overcome tumor resistance by enhancing the effector function of T-lymphocytes with immunotherapies that target the CTLA-4 and PD-1/PD-L1 checkpoint pathways (10,11). Preliminary reports indicated favorable effects of chemoembolic therapy on T-cell infiltration and enhanced tumor-associated antigen release (12). Moreover, pH buffering with sodium bicarbonate prior to TACE has been shown to restore peritumoral immune cell infiltration (13). There is, however, a paucity of data regarding possible differences between clinically used chemoembolic materials on the immune response. Since using a certain TACE regimen possibly modifies the study outcome itself, this lack of information may result in a confounding of data across ongoing and future clinical trials combining TACE with immunotherapy. A better understanding of this TACE regimen–dependent immunogenicity is therefore needed.

This study was designed to characterize the effects of commonly used TACE regimens on immune cell recruitment and immune checkpoint marker expression using a VX2 rabbit liver tumor model.

MATERIALS AND METHODS

Experimental Design

Male adult New Zealand white rabbits (2.5–4 kg, Charles River Laboratories, Boston, Massachusetts) were used according to the institutional animal care and use committee protocol (Yale University IACUC, protocol number 20100). Twenty-four rabbits were injected with VX2 tumor chunks into the left liver lobe via median laparotomy, as previously described (14,15). Tumors were grown for 14–21 days until baseline contrast-enhanced magnetic resonance imaging (n = 18) or computed tomography (CT) (n = 6) was performed, and a delineated solitary tumor lesion of 1–2 cm was detectable. Subsequently, rabbits were randomly assigned to 7 groups (n = 3 per group) undergoing LRT as follows: (*a*) bicarbonate infusion without embolization, (*b*) cTACE using ethiodized oil, DEE-TACE with either (*c*) idarubicin-eluting Oncozene microspheres or (*d*) doxorubicin-eluting Lumi beads. To each TACE treatment arm (*a*–*d*), a group of animals (n = 3 per group) treated with additional bicarbonate infusion was added to evaluate the effect of pH modification on the immune response. Untreated rabbits (n = 3) served as controls. Randomization of the groups was generated using the standard = RAND () function in Microsoft Excel. Tissue was harvested 24 hours after treatment for histopathologic analysis of immediate changes in the TME (Fig 1; Fig E1, available online on the article's Supplemental Material page at www.jvir.org). The immunological long-term effects of TACE will be investigated in future studies.

TACE Procedure

A blunt dissection done in previously anesthetized rabbits allowed access to the right or left common femoral artery, as previously described (13–16). Briefly, a 3-F vascular groin sheath (Cook Medical, Bloomington, Indiana) was used to advance a 2-F microcatheter (JB1 catheter; Cook) into the celiac axis followed by a celiac arteriogram to delineate the blood supply of the liver. The target lesion and feeding vessels were identified using either digital subtraction angiography or dual-phase cone-beam CT (C-arm; Allura Clarity FD20, XtraVision Release 8.2; Philips, Best, The Netherlands). After initial mapping, a

0.014-inch guide wire (Transend; Boston Scientific, Marlborough, Massachusetts) was used to selectively catheterize the tumor-feeding artery. Embolization endpoints were defined as complete blood flow stasis. Upon completion of the procedure, the microcatheter was removed, the common femoral artery was ligated, and the cut-down was closed.

Conventional TACE Protocol

Conventional TACE was performed according to standard protocols and as previously described (14,16). In brief, upon the placement of the catheter under fluoroscopic monitoring, a water-in-oil emulsion containing 1.25 mg/mL solution of doxorubicin hydrochloride (HCl) (RPI, Mount Prospect, Illinois) mixed in a ratio of 1:2 with ethiodized oil (Lipiodol; Guerbet, Villepinte, France) to a total volume of 0.2–0.3 mL was slowly delivered, depending on the tumor size, vascular supply, and arterial patency. After rinsing the catheter with saline, 0.3–0.4 mL of 100–300 μm trisacryl gelatin microspheres (Embosphere; Merit Medical, South Jordan, Utah) diluted in a ratio of 1:4 with Omnipaque 350 contrast agent (Amersham Health, Princeton, New Jersey) were injected until complete stagnation of the blood flow was confirmed by intraprocedural fluoroscopy.

DEE-TACE Protocol

For the first DEE-based regimen, 40-μm Oncozene microspheres (Varian, Palo Alto, California) were loaded with 15 mg of idarubicin HCl solution (Idamycin PFS; Pfizer, New York City, New York), and 3 mL of this suspension was diluted in 7.5 mL of contrast agent and 7.5 mL of sterile water. Following this, a volume of 0.3–0.5 mL was slowly infused into the previously placed catheter until complete blood flow stasis was achieved (16).
For the second DEE-based regimen, 40–90-μm radiopaque Lumi beads (Boston Scientific, Maple Grove, Minnesota) were loaded with doxorubicin HCl solution. After diluting the sedimented beads in contrast agent to a final concentration of 1.25 mg/mL, 0.2–0.4 mL of this solution was infused into the tumor-feeding artery until stasis was achieved (16). Both DEE-loading protocols were performed according to the manufacturers' instructions.

Bicarbonate Administration

In the animals undergoing bicarbonate-buffered TACE treatment, the tumor-feeding artery was infused with 5 mL of clinically used 4% sodium bicarbonate (Neut; Hospira, Lake Forest, Illinois) over 5 minutes before embolization as previously described (13,16). Next, the catheter was flushed to prevent clotting. The consecutive application of embolic materials is hypothesized to prevent the bicarbonate from being washed out of the tumor tissue. Rabbits receiving bicarbonate infusion without embolization were infused exclusively with 5 mL of 4% sodium bicarbonate over 5 minutes.

Tissue Collection and Processing

All animals were sacrificed by intravenous infusion of Euthasol (0.5 mL/kg) 24 hours following LRT (treatment groups) or the imaging session (control group). Necropsy was performed immediately to harvest the tumor and peritumoral liver parenchyma. The samples were sectioned (3–5 mm), fixed overnight at 4°C in 10% buffered formalin (Avantik Biogroup, Pine Brook, New Jersey), and embedded in paraffin.

Histopathologic Analysis and Immunohistochemical Staining

Paraffin-embedded blocks were cut into 2-μm slices and processed for immunohistochemical staining as described in detail in Appendix A (available online at www.jvir.org). A board-certified, gastrointestinal-subspecialized liver pathologist (X.Z.) with clinical and research focus on liver cancer and >10 years of clinical experience in this field verified the specificity of the primary antibodies in rabbit tissue (Table 1; Fig E2, available online at www.jvir.org). Hematoxylin and eosin staining, performed according to standard protocols, allowed a histopathologic evaluation of tumor necrosis and morphology.

Histopathologic Quantification and Validation of the Image Analysis Algorithm

All slides were digitized using a Leica Aperio Scanscope XT scanner (Leica Biosystems Imaging Inc., Vista, California) at 20× objective magnification. The tumor core was defined as approximately half of the tumor volume, and the tumor edge as the region excluded from the core (17). The positive pixel count algorithm V9 by Aperio ImageScope (v12.3) software enabled the quantification of immune cell distribution of cluster of differentiation 3^+ ($CD3^+$) T-cells and human leukocyte antigen DR type ($HLA\text{-}DR^+$) antigen-presenting cells (APCs) and the CTLA-4, PD-1, and PD-L1 immune checkpoint marker expression. Four representative hotspot areas (size, 220,090 μm^2) in the tumor border and core area were annotated manually and analyzed for each marker in each tumor. The mean positive pixel count was divided by the size of the area to calculate the average percentage cell positivity per μm^2 hotspot area separately for peritumoral and intratumoral regions. To ensure reproducibility, the process was repeated by a second reader (A.M.B.) in a subset of the data (one tumor/group for each marker). Agreement between the 2 raters (X.Z. and A.M.B.) was assessed by means of the intraclass correlation coefficient 3 (18).

Statistical Analysis

The semiquantitative group size of n = 3 chosen in this study is comparable to previously published research in this area (19,20). A Kruskal-Wallis test was used for pairwise statistical comparisons (Prism8, GraphPad Software Inc., San Diego, California), followed by Benjamini, Krieger, and Yekutieli post-hoc analysis to control the false discovery rate. *P* values <.05 were considered statistically significant. Intraclass correlation coefficients 3 were calculated in Python (v.3.8) using the Pingouin library (v.0.3.11).

RESULTS

Intra-arterial Procedures and Digital Histopathologic Evaluation

Intra-arterial procedures were technically successful, and embolization endpoints were reached in all animals (100%). Representative histopathologic data are presented in Figure 2a, b. Average percentage cell positivity is summarized as mean ± SEM in Table 2 and Figure 3, with corresponding statistical analysis displayed in Table 3. High interreader agreement ($P \leq .0001$) between the 2 raters on a subset of the data demonstrated the reproducibility of the results (Fig E3 and Table E1, available online at www.jvir.org).

Untreated Tumor Controls

Untreated tumors demonstrated low immune cell infiltration in the tumor edge (CD3, 0.25 ± 0.06; HLA-DR, 0.57 ± 0.25) and core area (CD3, 0.37± 0.09; HLA-DR, 0.63 ± 0.05) (Fig 3a, b). In contrast, the expression of the immune checkpoint markers in the tumor edge (CTLA-4, 1.72 ± 0.17; PD1, 0.97 ± 0.1; PD-L1, 0.84 0.06) and core area (CTLA-4, 1.78 ± 0.16; PD1, 1.3 ±0.23; PD-L1, 1.09 ± 0.2) was the highest among all the groups (Fig 3c, d, e).

Treatment with Bicarbonate Infusion

Treatment with bicarbonate infusion alone did not restore this low peritumoral (CD3, 0.16 ± 0.1; HLA-DR, 0.35 ± 0.16) and intratumoral (CD3, 0.26 ± 0.08; HLA-DR, 0.53 ± 0.07) immune cell infiltration (Fig 3a, b). The analyzed immune checkpoint markers were downregulated, but only the peritumoral CTLA-4 expression was significantly reduced compared with the controls (0.49 ± 0.1 vs 1.72 ± 0.17, $P = .0089$) (Fig 3c1).

Treatment with cTACE

Treatment with cTACE generated significantly decreased $CD3^+$ T-cell (0.03 ± 0.02 vs 0.37 ± 0.09, $P < .0001$) and $HLA\text{-}DR^+$ APC (0.29 ± 0.14 vs 0.63 ± 0.05, $P = .0379$) recruitment in the tumor core compared with the controls (Fig 3a2, b2). Moreover, cTACE treatment significantly reduced the checkpoint marker expression in the tumor edge (CTLA-4, 0.27 ± 0.18 vs 1.72 ± 0.17, $P < .0001$; PD-L1, 0.21 ± 0.06 vs 0.84 ± 0.06, $P < .0001$) and core area (CTLA-4, 0.02 ± 0.0 vs 1.78 ± 0.16, $P < .0001$; PD-1, 0.0 0.0 vs 1.3 ± 0.23, $P < .0001$; PD-L1, 0.3 ± 0.11 vs 1.09 ± 0.2, $P = .0002$) compared with untreated tumors (Fig 3c, d, e).

Treatment with Idarubicin-Eluting Oncozene Microspheres

The Oncozene-microsphere TACE treatment regimens did not significantly alter tumor-infiltrating $CD3^+$ T-cells and $HLA\text{-}DR^+$ APCs compared with the controls (Table 2, Table 3a, b, Fig 3a, b). However, the expression of the immune checkpoint markers in the tumor edge (CTLA-4, 0.22 ± 0.12 vs 1.72 ± 0.17, $P < .0001$; PD-1, 0.0 ± 0.0 vs 0.97 ± 0.1, $P < .0001$; PD-L1, 0.34 ± 0.1 vs 0.84 ± 0.06, $P = .0046$) and core area (CTLA-4, 0.02 ± 0.0 vs 0.0 1.78 ± 0.16, $P < .0001$; PD-1, 0.0 ± 0.0 vs 1.3 ± 0.23, $P < .0001$; PD-L1, 0.29 ± 0.09 vs 1.09 ± 0.2, $P = .0002$) was significantly reduced compared with the controls (Fig 3c, d, e).

Treatment with Doxorubicin-Eluting Lumi Beads

The bicarbonate-buffered Lumi-bead group was characterized by the highest intratumoral immune cell infiltration across the treatment arms (CD3, 0.49 ± 0.3, HLA-DR: 1.02 ± 0.27) (Fig 3a2, b2). Lumi-bead TACE enabled significantly more intratumoral immune cell infiltration than cTACE (CD3, 0.33 ± 0.2 vs 0.03 ± 0.1 0.02, $P = .0003$; HLA-DR, 0.78 ± 0.1 vs 0.29 ± 0.14, $P < .0001$) and Oncozene-microsphere TACE (HLA-DR, 0.78 ± 0.1 vs 0.48 ± 0.08, $P = .0113$) (Fig 3a2, b2). Additionally, Lumi-bead-TACE–treated tumors demonstrated significantly higher immune checkpoint marker expression in the tumor core compared with cTACE (CTLA-4, 0.6 ± 0.31 vs 0.02 ± 0.0, $P < 0.0001$; PD-1, 0.5 ± 0.1 vs 0.0 ± 0.0, $P < .0001$; PD-L1, 0.86 ± 0.24 vs 0.3 ± 0.11, $P = .002$) and Oncozene-microsphere

TACE (CTLA-4, 0.6 ± 0.31 vs 0.02 ± 0.0, P <.0001; PD-1, 0.5 ± 0.1 vs 0.0 ± 0.0, P <.0001; PD-L1, 0.86 ± 0.24 vs 0.29 ± 0.09, P = .0021) (Fig 3c2, d2).

Combined Treatment of Bicarbonate with Different TACE Modalities

The combined use of bicarbonate with different TACE modalities induced intratumoral $CD3^+$ T-cell and HLA-DR^+ APC recruitment, whereas only the combined use of cTACE with Lipiodol and bicarbonate enabled significantly higher intratumoral $CD3^+$ T-cell infiltration compared with unbuffered cTACE (0.26 ± 0.1 vs 0.03 ± 0.02, P = .0003) (Fig 3a2, b2). The downregulation of CTLA-4 and PD-1 characterized further combined pH-buffered TACE compared with the unbuffered treatment groups (Table 2, Fig 3c, d). The peritumoral PD-1 expression in the bicarbonate-buffered cTACE (0.0 ± 0.0 vs 0.43 ± 0.08, P = .0003) and intratumoral PD-1 expression in the pH-buffered LUMI-bead group (0.0 ± 0.0 vs 0.5 ± 0.1, P < .0001) was significantly reduced (Fig 3d). PD-L1 was modified reversely, being significantly more highly expressed in the bicarbonate-buffered cTACE group in the tumor border (0.5 ± 0.0 vs 0.21 ± 0.06, P = .0003) and core area (1.0 ± 0.0 vs 0.3 ± 0.11, P = .0007) compared to the unbuffered group (Fig 3e).

DISCUSSION

The present study data highlights substantial TACE regimen–dependent differences in evoked tumor immunogenicity. TACE with doxorubicin-eluting Lumi beads was identified as the most potent regimen capable of inducing immune cell recruitment and immune checkpoint marker expression in the tumor core. The addition of neoadjuvant bicarbonate administration demonstrated the most pronounced effect on the cTACE group and resulted in a significant increase in intratumoral T-cell infiltration.

Untreated liver tumors are characterized by mild immune cell infiltration and acidosis, leading to the hypoxia-inducible factor 1-α–induced upregulation of immune checkpoints (2,3). Previously, the therapeutic buffering of the peritumoral extracellular pH has been shown to make the tumor more susceptible to antitumor immunity (13,21). Nevertheless, bicarbonate infusion alone did not sufficiently restore the intratumoral immune response, and immune checkpoints remained highly expressed.

Previous studies (13) have already demonstrated the ability of cTACE to neutralize tumor-induced acidity and to restore an efficient immune response. Despite those encouraging results, our findings demonstrate that tumors treated with cTACE alone exhibit comparatively low immune cell infiltration. TACE with Lipiodol might induce an initial “proton trapping,” preventing immune cells from infiltrating the tumor.

DEE-TACE with idarubicin-eluting Oncozene microspheres induced low regional $CD3^+$ T-cell and HLA-DR^+ APC recruitment and downregulated immune checkpoint marker expression. Idarubicin is an analog of doxorubicin, the most used anthracycline antibiotic with antineoplastic activity (22). The use of idarubicin is frequently justified by the absence of the methoxy group on the left phenyl ring and hydroxyl group on the acetyl group, which increases idarubicin’s fat solubility and cellular uptake (22,23). Since idarubicin has the highest toxicity index for HCC, theoretically, its use may result in more efficient tumor

destruction (23). Additionally, previous observations (8,24) have shown that Oncozenes as small microspheres induce distal tumor vessel penetration and potentiate tumor necrosis and antitumor tissue effects. However, none of these potentially beneficial characteristics translated into increased immunogenicity in the tested Oncozene-microsphere groups. The chemical structure of the drug carrier itself, as a negatively charged, biocompatible, non-resorbable hydrogel microsphere coated with an inorganic polyphosphazene polymer, may be one of the reasons for the observed findings.

The treatment with Lumi beads restored intratumoral immune cell accumulation and showed the overall highest expression of immune checkpoint markers across the tested treatment regimens. Lumi-bead microspheres are sulfonate-modified polyvinyl alcohol hydrogel microbeads (9). This different composition of the underlying material of Lumi beads, along with physical parameters, such as being a static foreign body compared to Lipiodol being a liquid embolic, may account for their higher immunogenicity.

These findings further reveal the ability of combined pH-buffered TACE treatment to induce $CD3^+$ T-cell infiltration, HLA-DR^+ APC recruitment, and downregulation of the PD-1 and CTLA-4 checkpoint marker expression. The increased presence of tumor-infiltrating lymphocytes in this group may conceivably enable interferon-γ signaling and explain the elevated PD-L1 expression in bicarbonate-buffered TACE (25). The additional bicarbonate administration had the most pronounced effect on cTACE, leading to restored intratumoral T-cell infiltration. This observation may be explained by Lipiodol's ability to penetrate small capillary vessels combined with the use of blocking microparticles in larger feeding arteries, therefore allowing for cTACE to retain bicarbonate in the tumoral tissues (8). As DEE-TACE targets comparably larger caliber vessels, bicarbonate may be exposed to washout from collateral perfusion, particularly if complete stasis is not achieved (8,9). Given that normalized extracellular pH is known to induce immune infiltration and to improve clinical responses to systemic immunotherapy, our data suggest that additional pH buffering may be particularly beneficial for cTACE in a scenario where intra-arterial therapy is combined with systemic immunotherapy (26).

This study had a number of limitations. These include the relatively small cohort size of 3 animals per group and the short follow-up period. However, as a proof-of-concept observation, it did show reproducible results. Even though the rabbit VX2 tumor model is a squamous cell carcinoma allograft model of nonhepatic origin, it has been validated as an immunocompetent model that is predictive of the TME encountered in human HCC and is widely used as a model for various intra-arterial drug delivery techniques (13–16,24,27). A model-related limitation is the inherent VX2 tumor aggressiveness, the frequently encountered central tumor necrosis at baseline, and a relatively wide range of tumor sizes across individuals (24,27,28). This may impact the overall assessment of immunological changes in the TME; however, this was accounted for by comparing different groups including control group animals. Since multimodal histopathologic data are difficult to collect in clinical populations, plausible conclusions about a possibly TACE regimen–dependent immunogenicity can only be drawn by preclinical studies like the present one. In addition, the comparability between Oncozene microspheres, Lumi beads, and cTACE is limited because of the different drug used in the Oncozene group. However, Oncozene

microspheres are industrially designed to bind and elute idarubicin in a standardized fashion, while no data exist to support the standard use of doxorubicin for this bead. Therefore, this study was intended to use clinically acceptable drug protocols for all TACE regimens rather than homogenizing drug type within the experimental groups. Although longitudinal outcomes were not investigated by this study design, our study endpoint may be ultimately too early for the DEE-treated groups to fully reveal their anti-tumoral drug effects as their highest parenchymal drug concentration is usually observed 3 days after embolization (29). This suggests that treatment effects in these groups were mainly caused by devascularization as a predominantly short-term therapeutic mechanism rather than by the chemotherapeutic agents. Although the methodology of digital immunopathologic characterization has been validated previously to determine the densities of stained cells, it should be noted that our analysis was spatially limited and represented a 2-dimensional snapshot of the tissue cut in multiple planes (30).

In conclusion, this preclinical study demonstrated significant differences between various types of chemoembolic regimens on the complex interplay between immunogenic potential and susceptibility to therapy with immune checkpoint inhibitors. The findings represent a framework for further experimental and clinical investigations to allow for standardized regimens before pursuing drug combination studies to avoid the confounding effects of suboptimal regimens.

Supplementary Material

Refer to Web version on PubMed Central for supplementary material.

ACKNOWLEDGMENTS

This study was funded by the Society of Interventional Oncology grant 19-001324 and National Institutes of Health grants R01 CA206180 and R01 EB023366. The content is solely the responsibility of the authors and does not necessarily represent the official views of the National Institutes of Health or Society of Interventional Oncology. The authors thank the Yale Liver Center Award (NIH P30 DK034989) Microscopy Core for their support with resources and expertise and thank Boston Scientific and Guerbet for providing materials for this study. Raw data were generated at the Department of Radiology and Biomedical Imaging, Yale School of Medicine. Derived data supporting the findings of this study are available from the corresponding author J.C. upon reasonable request.

A.M.Be., S.I., and M.G. report a travel grant from the Rolf W. Günther Foundation for Radiological Research. L.J.S. reports grants from the Leo-poldina Postdoctoral Fellowship and the Junior Clinician Scientist Program of the Berlin Institute of Health outside the submitted work. L.A.G. reports a travel grant from the Rolf W. Günther Foundation for Radiological Research and a scholarship from the German Academic Scholarship Foundation. M.L. is an employee and stockholder of Visage Imaging, Inc., receives funding from National Institutes of Health/ National Cancer Institute (R01 CA206180), and is a board member of Tau Beta Pi engineering honor society. D.C.M. is a consultant for Guerbet and Boston Scientific. J.C. reports grants from the National Institutes of Health, Society of Interventional Oncology, Yale Center for Clinical Investigation, and Rolf W. Günther Foundation for Radiological Research outside the submitted work and is a consultant for Bayer, Guerbet, Philips, and Boston Scientific. J.C. is a consultant for AstraZeneca. None of the other authors have identified a conflict of interest.

ABBREVIATIONS

APC	antigen-presenting cell
CT	computed tomography
cTACE	conventional transcatheter arterial chemoembolization

CTLA-4	cytotoxic T-lymphocyte–associated protein-4
DEE	drug-eluting embolic
HCC	hepatocellular carcinoma
HCl	hydrochloric acid
LRT	locoregional therapy
PD-1	programmed cell death protein-1
PD-L1	programmed cell death protein-1 ligand
TACE	transcatheter arterial chemoembolization
TME	tumor microenvironment

REFERENCES

1. Greten TF, Duffy AG, Korangy F. Hepatocellular carcinoma from an immunologic perspective. Clin Cancer Res 2013; 19:6678–6685. [PubMed: 24030702]
2. Huber V, Camisaschi C, Berzi A, et al. Cancer acidity: an ultimate frontier of tumor immune escape and a novel target of immunomodulation. Semin Cancer Biol 2017; 43:74–89. [PubMed: 28267587]
3. Calcinotto A, Filipazzi P, Grioni M, et al. Modulation of microenvironment acidity reverses anergy in human and murine tumor-infiltrating T lymphocytes. Cancer Res 2012; 72:2746–2756. [PubMed: 22593198]
4. Feng J, Yang H, Zhang Y, et al. Tumor cell-derived lactate induces TAZ-dependent upregulation of PD-L1 through GPR81 in human lung cancer cells. Oncogene 2017; 36:5829–5839. [PubMed: 28604752]
5. Heimbach JK, Kulik LM, Finn RS, et al. AASLD guidelines for the treatment of hepatocellular carcinoma. Hepatology 2018; 67:358–380. [PubMed: 28130846]
6. Llovet JM, Real MI, Moñtana X, et al. Arterial embolisation or chemoembolisation versus symptomatic treatment in patients with unresectable hepatocellular carcinoma: a randomised controlled trial. Lancet 2002; 359:1734–1739. [PubMed: 12049862]
7. Lo CM, Ngan H, Tso WK, et al. Randomized controlled trial of transarterial lipiodol chemoembolization for unresectable hepatocellular carcinoma. Hepatology 2002; 35:1164–1171. [PubMed: 11981766]
8. Song JE, Kim DY. Conventional vs drug-eluting beads transarterial chemoembolization for hepatocellular carcinoma. World J Hepatol 2017; 9:808–814. [PubMed: 28706579]
9. Lewis AL, Gonzalez MV, Lloyd AW, et al. DC bead: in vitro characterization of a drug-delivery device for transarterial chemoembolization. J Vasc Interv Rardiol 2006; 17:335–342.
10. Dai X, Wang S, Niu C, Ji B, Liu Y. Overview of current progress in immune checkpoint inhibitor therapy for advanced hepatocellular carcinoma. Technol Cancer Res Treat 2020; 19:1533033820947486.
11. Erinjeri JP, Fine GC, Adema GJ, et al. Immunotherapy and the interventional oncologist: challenges and opportunities—a Society of Interventional Oncology white paper. Radiology 2019; 292:25–34. [PubMed: 31012818]
12. Singh P, Toom S, Avula A, Kumar V, Rahma OE. The immune modulation effect of locoregional therapies and its potential synergy with immunotherapy in hepatocellular carcinoma. J Hepatocell Carcinoma 2020; 7: 11–17. [PubMed: 32104669]
13. Savic LJ, Doemel LA, Schobert IT, et al. Molecular MRI of the immune-metabolic interplay in a rabbit liver tumor model : a biomarker for resistance mechanisms in tumor-targeted therapy? Radiology 2020; 296: 575–583. [PubMed: 32633675]

14. Savic LJ, Schobert IT, Peters D, et al. Molecular imaging of extracellular tumor pH to reveal effects of locoregional therapy on liver cancer microenvironment. Clin Cancer Res 2020; 26:428–438. [PubMed: 31582517]
15. Geschwind JF, Artemov D, Abraham S, et al. Chemoembolization of liver tumor in a rabbit model: assessment of tumor cell death with diffusion-weighted MR imaging and histologic analysis. J Vasc Interv Rardiol 2000; 11:1245–1255.
16. Doemel LA, Santana JG, Savic LJ, et al. Comparison of metabolic and immunologic responses to transarterial chemoembolization with different chemoembolic regimens in a rabbit VX2 liver tumor model. Eur Radiol 2022; 32:2437–2447. [PubMed: 34718844]
17. Schmieder AH, Winter PM, Williams TA, et al. Molecular MR imaging of neovascular progression in the Vx2 tumor with αvβ3-targeted paramagnetic nanoparticles. Radiology 2013; 268:470–480. [PubMed: 23771914]
18. Shrout PE, Fleiss JL. Intraclass correlations: uses in assessing rater reliability. Psychol Bull 1979; 86:420–428. [PubMed: 18839484]
19. Keller S, Borde T, Brangsch J, et al. Assessment of the hepatic tumor extracellular matrix using elastin-specific molecular magnetic resonance imaging in an experimental rabbit cancer model. Sci Rep 2020; 10:20785.
20. Vossen JA, Buijs M, Geschwind JF, et al. Diffusion-weighted and Gd-EOB-DTPA-contrast-enhanced magnetic resonance imaging for characterization of tumor necrosis in an animal model. J Comput Assist Tomogr 2009; 33:626–630. [PubMed: 19638862]
21. Estrella V, Chen T, Lloyd M, et al. Acidity generated by the tumor microenvironment drives local invasion. Cancer Res 2013; 73: 1524–1535. [PubMed: 23288510]
22. Miller JP, Stoodley RJ. Studies directed towards anthracyclinone syntheses: the use of d-glucose as a chiral auxiliary in asymmetric Diels–Alder reactions. J Saudi Chem Soc 2013; 17:29–42.
23. Boulin M, Guiu S, Chauffert B, et al. Screening of anticancer drugs for chemoembolization of hepatocellular carcinoma. Anticancer Drugs 2011; 22:741–748. [PubMed: 21487286]
24. Borde T, Laage Gaupp F, Geschwind JF, et al. Idarubicin-Loaded ONCOZENE Drug-eluting bead chemoembolization in a rabbit liver tumor model: investigating safety, therapeutic efficacy, and effects on tumor microenvironment. J Vasc Interv Rardiol 2020; 31: 1706–1716.e1.
25. Garcia-Diaz A, Shin DS, Moreno BH, et al. Interferon receptor signaling pathways regulating PD-L1 and PD-L2 expression. Cell Rep 2017; 19: 1189–1201. [PubMed: 28494868]
26. Pilon-Thomas S, Kodumudi KN, El-Kenawi AE, et al. Neutralization of tumor acidity improves antitumor responses to immunotherapy. Cancer Res 2016; 76:1381–1390. [PubMed: 26719539]
27. Mostafa EM, Ganguli S, Faintuch S, Mertyna P, Goldberg SN. Optimal strategies for combining transcatheter arterial chemoembolization and radiofrequency ablation in rabbit VX2 hepatic tumors. J Vasc Interv Rardiol 2008; 19:1740–1748.
28. Virmani S, Harris KR, Szolc-Kowalska B, et al. Comparison of two different methods for inoculating VX2 tumors in rabbit livers and hind limbs. J Vasc Interv Rardiol 2008; 19:931–936.
29. Hong K, Khwaja A, Liapi E, Torbenson MS, Georgiades CS, Geschwind JF. New intra-arterial drug delivery system for the treatment of liver cancer: preclinical assessment in a rabbit model of liver cancer. Clin Cancer Res 2006; 12:2563–2567. [PubMed: 16638866]
30. Galon J, Mlecnik B, Bindea G, et al. Towards the introduction of the 'Immunoscore' in the classification of malignant tumours. J Pathol 2014; 232:199–209. [PubMed: 24122236]

RESEARCH HIGHLIGHTS

- Significant differences in T-cell recruitment and immune checkpoint marker expression were observed between the 3 tested chemoembolic transcatheter arterial chemoembolization (TACE) regimens using digital immunohistochemistry quantification.
- TACE with Lumi beads was identified as the single most potent regimen, capable of inducing intratumoral T-cell recruitment and immune checkpoint marker expression as compared with conventional TACE and Oncozene-microsphere TACE.
- Neoadjuvant bicarbonate infusion increased cluster of differentiation 3^+ T-cell infiltration with cTACE but had no significant effect on drug-eluting embolic-TACE using Oncozene microspheres or Lumi beads.

STUDY DETAILS

Study type:

Animal study

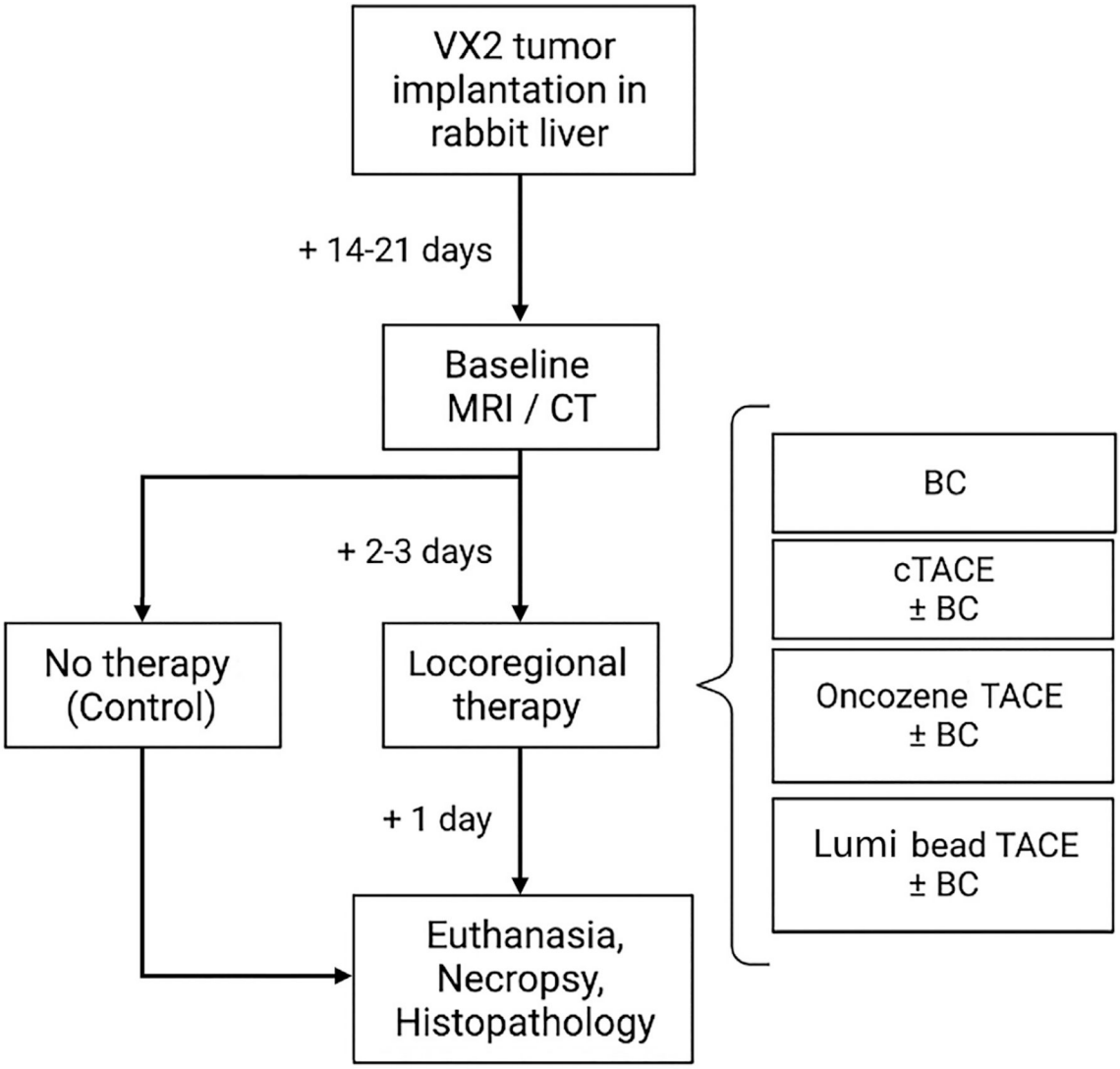

Figure 1.

Flowchart of the experimental study design. Twenty-four New Zealand white rabbits were implanted with VX2 tumors in the left liver lobe. The tumors were grown for 14–21 days until baseline magnetic resonance imaging (MRI) or computed tomography (CT) was performed. Next, 3 rabbits were euthanized and served as controls. The remaining 21 rabbits were assigned to 7 groups (n = 3 per group) undergoing locoregional therapy: bicarbonate infusion without embolization (BC), conventional transcatheter arterial chemoembolization (cTACE) with Lipiodol, drug-eluting embolic-TACE with either idarubicin-eluting Oncozene microspheres (40 μm) or doxorubicin-eluting Lumi beads (40–90 μm). For each therapy arm, a set of animals (n = 3) with additional bicarbonate infusion before TACE was added. After euthanasia, necropsy was performed and tissue was harvested for histopathologic analysis.

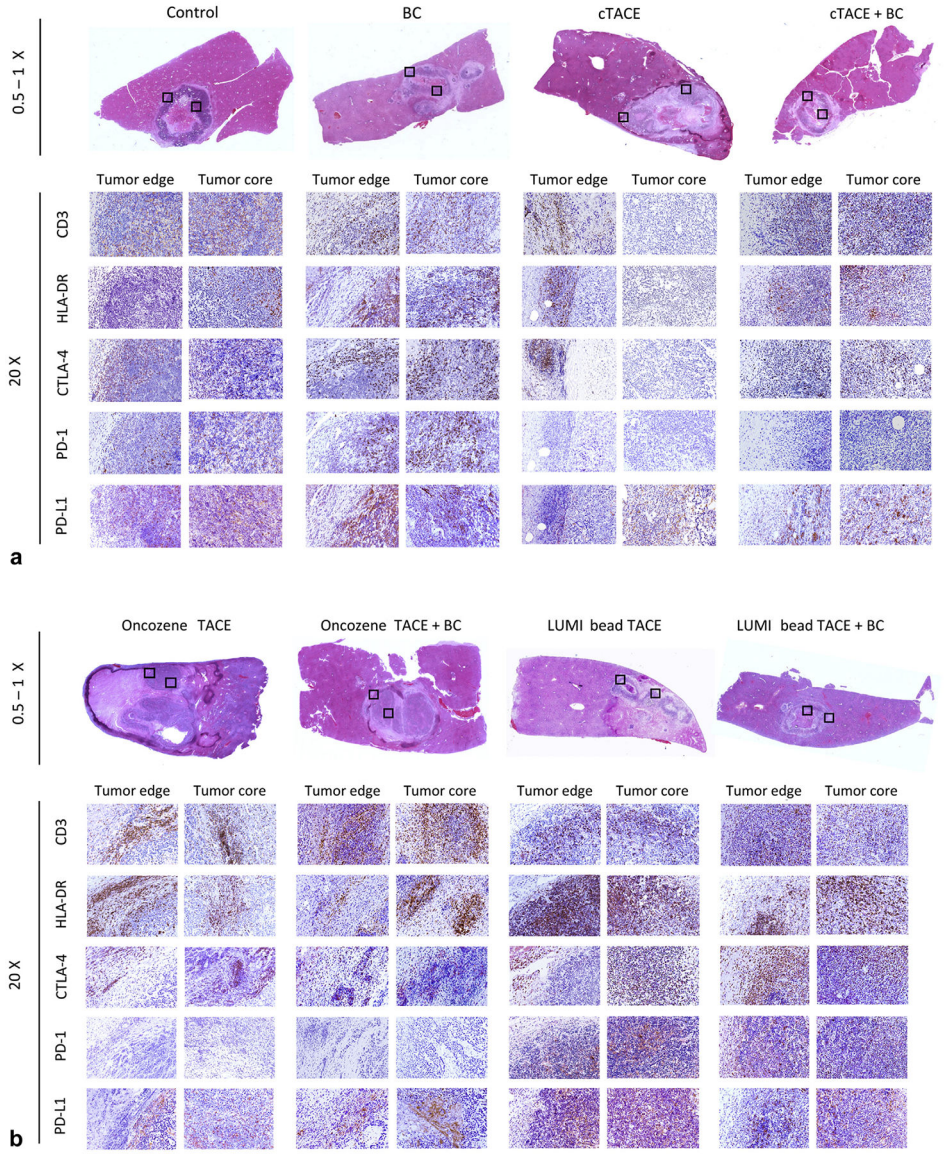

Figure 2.

(a, b) Histopathologic representation of the immune cell recruitment. Hematoxylin and eosin (0.5–1×) stainings (first row) indicate the regions in the tumor edge and core areas (boxed areas) chosen for magnification (20×) of immune stainings for cluster of differentiation 3 (CD3), human leukocyte antigen DR type (HLA-DR), cytotoxic T-lymphocyte–associated protein-4 (CTLA-4), programmed cell death protein-1 (PD-1), and PD-1 ligand (PD-L1) in the following rows across the control and treatment groups. BC = bicarbonate; cTACE: conventional transcatheter arterial chemoembolization; TACE = transcatheter arterial chemoembolization.

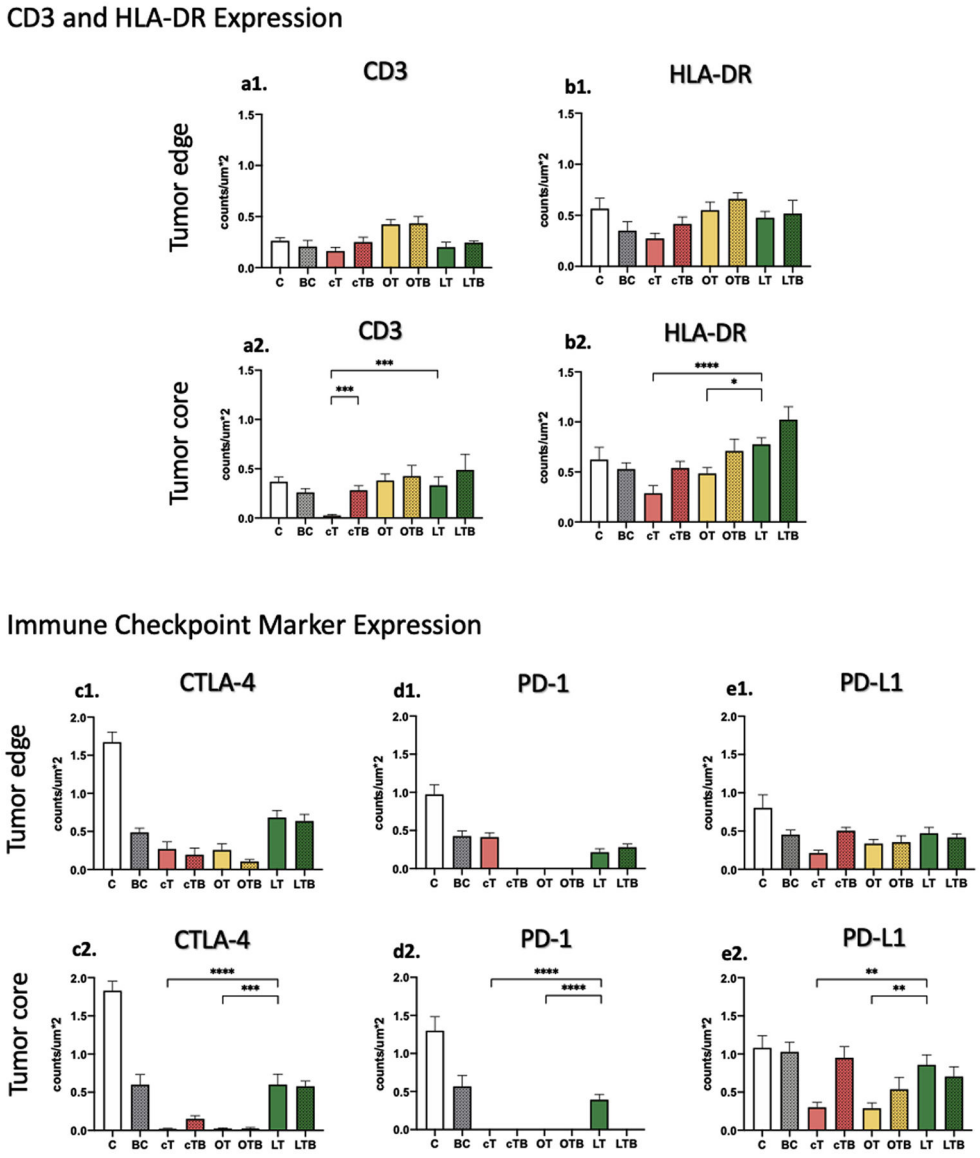

Figure 3.

Bar chart representation of percentage cell positivity per square micrometer hotspot area on immunohistochemistry stainings. Results of the experiments are summarized separately for the **(a1–e1)** tumor edge and **(a2–e2)** core areas as mean ± SEM. A Kruskal-Wallis test was used for pairwise statistical comparisons, and a *P* value <.05 was considered statistically significant (denoted with *, $P \leq .05$; **, $P \leq .001$; and ****, $P \leq .01$; ***, $P \leq .0001$). BC = bicarbonate; C = control; cT = conventional transcatheter arterial chemoembolization; cTB = conventional transcatheter arterial chemoembolization + bicarbonate; CTLA-4 = cytotoxic T-lymphocyte–associated protein-4; LT = LUMI-bead transcatheter arterial chemoembolization; LTB = LUMI-bead transcatheter arterial chemoembolization + bicarbonate; OT = Oncozene-microsphere transcatheter arterial chemoembolization; OTB, Oncozene-microsphere transcatheter arterial chemoembolization

+ bicarbonate; PD-1 = programmed cell death protein-1; PD-L1 = programmed cell death protein-1 ligand.

Table 1.

Primary Antibodies Used for Immunohistochemistry

mAb	Clone	Species	Dilution	Antigen retrieval buffer	Manufacturer	Catalog number
HLA-DR	LN3	Mouse	1:500	CB	BioLegend	327002
CD3	CD3-12	Rat	1:150	CB	Invitrogen	MA5-16622
CTLA-4	UMAB249	Mouse	1:200	TB	Origene	UM800141
PD-1	UMAB197	Mouse	1:200	EB	Origene	UM800089
PD-L1	UMAB229	Mouse	1:25	TB	Origene	UM800121

CB = citric buffer (pH: 6); CD = cluster of differentiation; CTLA-4 = cytotoxic T-lymphocyte–associated protein-4; EB = EDTA buffer (pH: 8); HLA-DR = human leukocyte antigen DR type; mAb = monoclonal antibody; PD-1 = programmed cell death protein-1; PD-L1 = programmed cell death protein-1 ligand; TB = Tris-EDTA buffer (pH: 9).

Table 2.

Average Cell Positivity (counts/μm^2) on Immunohistochemistry Stainings Summarized as Mean ± SEM.

Control	Bicarbonate							
	C	BC	cT	cTB	OT	OTB	LT	LTB
Tumor edge								
CD3	0.25 ± 0.06	0.16 ± 0.1	0.16 ± 0.01	0.25 ± 0.1	0.42 ± 0.05	0.43 ± 0.01	0.2 ± 0.1	0.25 ± 0.01
HLA-DR	0.57 ± 0.25	0.35 ± 0.16	0.27 ± 0.09	0.39 ± 0.12	0.55 ± 0.14	0.66 ± 0.09	0.48 ± 0.1	0.52 ± 0.17
CTLA-4	1.72 ± 0.17	0.49 ± 0.1	0.27 ± 0.18	0.19 ± 0.16	0.22 ± 0.12	0.1 ± 0.03	0.68 ± 0.15	0.64 ± 0.15
PD-1	0.97 ± 0.1	0.48 ± 0.1	0.43 ± 0.08	0.0 ± 0.0	0.0 ± 0.0	0.0 ± 0.0	0.21 ± 0.1	0.32 ± 0.04
PD-L1	0.84 ± 0.06	0.45 ± 0.04	0.21 ± 0.06	0.5 ± 0.0	0.34 ± 0.1	0.35 ± 0.12	0.43 ± 0.16	0.42 ± 0.03
Tumor core								
CD3	0.37 ± 0.09	0.26 ± 0.08	0.03 ± 0.02	0.26 ± 0.1	0.32 ± 0.07	0.43 ± 0.01	0.33 ± 0.2	0.49 ± 0.3
HLA-DR	0.63 ± 0.05	0.53 ± 0.07	0.29 ± 0.14	0.54 ± 0.1	0.48 ± 0.08	0.7 ± 0.18	0.78 ± 0.1	1.02 ± 0.27
CTLA-4	1.78 ± 0.16	0.7 ± 0.3	0.02 ± 0.0	0.15 ± 0.09	0.02 ± 0.0	0.03 ± 0.02	0.6 ± 0.31	0.58 ± 0.01
PD-1	1.3 ± 0.23	0.7 ± 0.28	0.0 ± 0.0	0.0 ± 0.0	0.0 ± 0.0	0.0 ± 0.0	0.5 ± 0.1	0.0 ± 0.0
PD-L1	1.09 ± 0.2	1.02 ± 0.21	0.3 ± 0.11	1.0 ± 0.0	0.29 ± 0.09	0.54 ± 0.25	0.86 ± 0.24	0.7 ± 0.1

BC = bicarbonate; C = control; cT = conventional transcatheter arterial chemoembolization; CD = cluster of differentiation; cTB = conventional transcatheter arterial chemoembolization + bicarbonate; CTLA-4 = cytotoxic T-lymphocyte–associated protein-4; HLA-DR = human leukocyte antigen DR type; LT = LUMI-bead transcatheter arterial chemoembolization; LTB = LUMI-bead transcatheter arterial chemoembolization + bicarbonate; OT = Oncozene-microsphere transcatheter arterial; OTB = Oncozene-microsphere transcatheter arterial chemoembolization + bicarbonate; PD-1 = programmed cell death protein-1; PD-L1 = programmed cell death protein-1 ligand.

Table 3.

Statistical Analysis of Immunohistochemistry Staining Quantification.

a: CD3	**Tumor edge**							
	C	**BC**	**cT**	**cTB**	**OT**	**OTB**	**LT**	**LTB**
Tumor core								
C		ns	ns	ns	ns	ns	ns	ns
BC	ns		ns	ns	0.0017	0.0040	ns	ns
cT	<0.0001	0.0004		ns	0.0002	0.0006	ns	ns
cTB	ns	ns	0.0003		ns	ns	ns	ns
OT	ns	ns	<0.0001	ns		ns	0.0017	ns
OTB	ns	ns	<0.0001	ns	ns		0.0040	ns
LT	ns	ns	0.0003	ns	ns	ns		ns
LTB	ns	ns	<0.0001	ns	ns	ns	ns	
b: HLA-DR	**Tumor edge**							
	C	**BC**	**cT**	**cTB**	**OT**	**OTB**	**LT**	**LTB**
Tumor core								
C		ns	ns	ns	ns	ns	ns	ns
BC	ns		ns	ns	ns	ns	ns	ns
cT	0.0379	ns		ns	ns	0.0005	ns	ns
cTB	ns	ns	ns		ns	ns	ns	ns
OT	ns	ns	ns	ns		ns	ns	ns
OTB	ns	ns	0.0048	ns	ns		ns	ns
LT	ns	ns	<0.0001	ns	0.0113	ns		ns
LTB	ns	0.0099	<0.0001	0.0087	0.0012	ns	ns	
c: CTLA-4	**Tumor edge**							
	C	**BC**	**cT**	**cTB**	**OT**	**OTB**	**LT**	**LTB**
Tumor core								
C		0.0089	<0.0001	<0.0001	<0.0001	<0.0001	0.0570	0.0334
BC	ns		0.0649	0.0247	0.0365	0.0053	ns	ns
cT	<0.0001	<0.0001		ns	ns	ns	0.0052	0.0117
cTB	0.0010	ns	ns		ns	ns	0.0025	0.0054

a: CD3	Tumor edge							
	C	BC	cT	cTB	OT	OTB	LT	LTB
OT	<0.0001	<0.0001	ns	ns		ns	0.0030	0.0071
OTB	<0.0001	0.0002	ns	ns	ns		0.0004	0.0009
LT	ns	ns	<0.0001	ns	<0.0001	0.0003		ns
LTB	ns	ns	<0.0001	0.0310	<0.0001	<0.0001	ns	
d: PD-1	**Tumor edge**							
	C	**BC**	**cT**	**cTB**	**OT**	**OTB**	**LT**	**LTB**
Tumor core								
C		ns	ns	<0.0001	<0.0001	<0.0001	0.0042	0.0387
BC	ns		ns	<0.0001	<0.0001	<0.0001	ns	ns
cT	<0.0001	<0.0001		0.0003	0.0003	0.0003	ns	ns
cTB	<0.0001	<0.0001	ns		ns	ns	0.0014	0.0004
OT	<0.0001	<0.0001	ns	ns		ns	0.0014	0.0004
OTB	<0.0001	<0.0001	ns	ns	ns		0.0014	0.0004
LT	ns	ns	<0.0001	<0.0001	<0.0001	<0.0001		ns
LTB	<0.0001	<0.0001	ns	ns	ns	ns	<0.0001	
e: PD-L1	**Tumor edge**							
	C	**BC**	**cT**	**cTB**	**OT**	**OTB**	**LT**	**LTB**
Tumor core								
C		ns	<0.0001	ns	0.0046	0.0088	ns	ns
BC	ns		0.0030	ns	ns	ns	ns	ns
cT	0.0002	0.0001		0.0003	ns	ns	0.0078	0.0091
cTB	ns	ns	0.0007		ns	ns	ns	ns
OT	0.0002	0.0001	ns	0.0007		ns	ns	ns
OTB	0.0216	0.0233	ns	ns	ns		ns	ns
LT	ns	ns	0.0020	ns	0.0021	ns		ns
LTB	ns	ns	0.0186	ns	0.0189	ns	ns	

Note–For each surface marker (**a**: CD3, **b**: HLA-DR, **c**: CTLA-4, **d**: PD-1, and **e**: PD-L1) data are summarized separately for the tumor edge (right upper fields) and tumor core (left lower fields) area. A Kruskal-Wallis test was used for pairwise statistical comparisons, and a *P* value <.05 was considered statistically significant. BC = bicarbonate; C = control; CD = cluster of differentiation; cT = conventional transcatheter arterial chemoembolization; cTB = conventional transcatheter arterial chemoembolization + bicarbonate; CTLA-4 = cytotoxic T-lymphocyte–associated protein-4; HLA-DR = human leukocyte antigen DR type; LT = LUMI-bead transcatheter arterial chemoembolization; LTB = LUMI-bead transcatheter arterial chemoembolization + bicarbonate; ns = not significant; OT = Oncozene-microsphere transcatheter arterial chemoembolization; OTB = Oncozene-microsphere transcatheter arterial chemoembolization + bicarbonat; PD-1 = programmed cell death protein-1; PD-L1 = programmed cell death protein-1 ligand.